Secrecy outage analysis of double shadowed Rician channels

Y. Ai✉, L. Kong and M. Cheffena

The double shadowed Rician model was recently proposed to describe some realistic physical signal propagation phenomena, where a Rician faded signal is impacted by cascaded shadowing processes. In this letter, we study the outage performance of the double shadowed Rician model. More specifically, we investigate the impact of two different shadowing processes on the secrecy performance by deriving novel and exact expressions for secrecy outage performance metrics. The obtained results reveal the following physical implications: 1) when a Rician faded signal undergoes line-of-sight (LoS) shadowing, which is futher cascaded by another round of composite shadowing, the latter form of shadowing imposes larger impact on the secrecy performance; 2) the widely investigated concept of "protected zone" to improve the secrecy performance should not be limited to the legitimate transmitter but also extended to the legitimate receiver due to the adverse shadowing effect cased by objects in its vicinity; and 3) the rate of outage performance degradation grows larger as the shadowings become severer.

Introduction: Physical layer security (PLS) has been widely considered as a promising paradigm to enhance communication security against eavesdropping in wireless systems [1]. The secrecy performance analysis of different communication setups over different shadowing/fading conditions such as double Rayleigh, generalized-Gamma, κ-μ, and Fisher-Snedecor $\mathcal{F}$, etc., have been investigated in [2–5] and the references therein. On the other hand, the emerging communication use cases greatly expand the conventional propagation environments to all sorts of new scenarios including, but not limited to, Internet of Things (IoT), body area network (BAN), drone communications, and vehicular network, etc [2]. A new communication scenario often implies new physical propagation phenomena, which might require to develop new mathematical models to correctly describe the propagation phenomena.

Recently, the double shadowed Rician model was developed in [6] to underpin some realistic signal reception scenarios, where a Rician faded signal undergoes line-of-sight (LoS) shadowing followed by another round of composite shadowing. Physically, this may arise when the dominant LoS signal power between the transmitter and receiver is subject to varying levels of shadowing while further shadowing of the received power (combined LoS and multipath components) occurs due to obstacles moving around it [6]. In this letter, we study the secrecy performance over the double shadowed Rician channel by deriving exact expressions for the secrecy outage probability (SOP) and probability of non-zero secrecy capacity (PNZSC).

Channel and system models: We consider the classic Wyner wiretap model: a source node (*S*) equpped with a directional antenna tries to transmit secret information to a desired destination node (*D*) over the main channel while an illegitimate eavesdropper (*E*) attempts to intercept the messages by decoding its received signals from the wiretap channel. It is assumed that both channels experience the independent but not necessarily identical double shadowed Rician fading.

With the signal envelop following double shadowed Rician model, the probability distribution function (PDF) of the instantaneous signal-to-noise ratio (SNR) can be written as [6]

$$f_\gamma(x)=\frac{\overline{\gamma}^{m_s}m_s(m_s-1)^{m_s}(1+k)}{[x(1+k)+(m_s-1)\overline{\gamma}]^{m_s+1}}\cdot\left(\frac{m_d}{m_d+k}\right)^{m_d}\cdot{}_2F_1\left(m_d,m_s+1;1;\frac{k(1+k)x}{(m_d+k)[x(1+k)+(m_s-1)\overline{\gamma}]}\right), \quad (1)$$

where the parameters m_d and m_s indicate the shadowing severity of the first and second rounds of shadowing processes (the lower value indicates more severe shadowing), respectively; k is the Rician k parameter, $\overline{\gamma}$ represents the corresponding average SNR, and ${}_2F_1(\cdot,\cdot;\cdot;\cdot)$ denotes the Gauss hypergeometric function [7, Eq. (9.10)].

The cumulative distribution function (CDF) of the SNR γ follows immediately from its relationship with PDF as

$$F_\gamma(x)=\sum_{p=0}^{\infty}A_p\cdot G_{2,2}^{1,2}\left(\frac{x(1+k)}{(m_s-1)\overline{\gamma}}\middle|\begin{matrix}1,1-m_s\\ p+1,0\end{matrix}\right), \quad (2)$$

where $G_{p,q}^{m,n}\left(x\middle|\begin{matrix}\mathbf{a}_p\\ \mathbf{b}_q\end{matrix}\right)$ is the Meijer G-function [7, Eq. (9.343)] and

$$A_p=\left(\frac{m_d}{m_d+k}\right)^{m_d}\left(\frac{k}{m_d+k}\right)^{p}\frac{(m_d)_p(p+1)_{m_s}\Gamma(p+2)}{\Gamma(m_s)\Gamma(p+2)\Gamma(p+1)\Gamma(p+m_s+1)}, \quad (3)$$

with $(x)_n$ being the Pochhammer symbol [7, p. xli].

In the following, we denote γ_D and γ_E as the instantaneous SNRs of the main and wiretap channels, respectively. Furthermore, the main channel is described by the parameters m_{d1}, m_{s1}, k_1, and $\overline{\gamma}_1$; and the wiretap channel is determined by the parameters m_{d2}, m_{s2}, k_2, and $\overline{\gamma}_2$.

SOP analysis: The instantaneous secrecy capacity of the considered wiretap model is defined as [8]

$$C_s(\gamma_D,\gamma_E)=\max\{\ln(1+\gamma_D)-\ln(1+\gamma_E),0\}. \quad (4)$$

The SOP is defined as the probability that the instantaneous secrecy capacity $C_s(\gamma_D,\gamma_E)$ falls under a predefined secrecy rate R_s, i.e., [5]

$$SOP=\Pr\left[\gamma_D<\Theta\gamma_E+\Theta-1\right]=\int_0^\infty F_{\gamma_D}(\Theta x+\Theta-1)\cdot f_{\gamma_E}(x)\,dx, \quad (5)$$

where $\Theta=\exp(R_s)>1$.

Applying the Parseval's formula for Mellin transform [9, Cor. 12.1], the SOP in (5) can be rewritten as the following contour integral:

$$SOP=\frac{1}{2\pi j}\int_{\mathcal{L}_1}\mathcal{M}[F_{\gamma_D}(\Theta x+\Theta-1),1-s]\cdot\mathcal{M}[f_{\gamma_E}(x),s]\,ds, \quad (6)$$

where $\mathcal{L}_1$ is the integration path from $c-j\infty$ to $c+j\infty$ with c being a constant, and $\mathcal{M}[f(x),s]$ is the Mellin transform of $f(x)$ [9, Chpt. 8.2].

We first solve the Mellin transform $\mathcal{M}[F_{\gamma_D}(\Theta x+\Theta-1),1-s]$. Expressing the Meijer G-funtion in the CDF (2) in terms of Mellin-Barnes type contour integral [7, Eq. (9.30)], we can obtain

$$\mathcal{M}[F_{\gamma_D}(\Theta x+\Theta-1),1-s]=\int_0^\infty x^{-s}F_{\gamma_D}(\Theta x+\Theta-1)\,dx=\sum_{p=0}^{\infty}\frac{A_p}{2\pi j}\cdot\int_{\mathcal{L}_2}\frac{\Gamma(p+1+\xi)\left[\frac{1+k_1}{(m_{s1}-1)\overline{\gamma}_1}\right]^{-\xi}}{\Gamma(1-\xi)[\Gamma(-\xi)\Gamma(m_{s1}-\xi)]^{-1}}\cdot\int_0^\infty\frac{x^{-s}}{(\Theta x+\Theta-1)^{\xi}}\,dx d\xi, \quad (7)$$

where $\mathcal{L}_2$ is some contour that separates the poles of $\Gamma(-\xi)$ from those of $\Gamma(1+p+\xi)$. The inner integral in (7) can be solved with the help of [7, Eq. (3.194.3)] as

$$\int_0^\infty x^{-s}(\Theta x+\Theta-1)^{-\xi}\,dx=\frac{\Gamma(1-s)\Gamma(s+\xi-1)}{\Gamma(\xi)(\Theta-1)^{\xi}}\cdot\left(\frac{\Theta}{\Theta-1}\right)^{s-1}. \quad (8)$$

Substituting (8) into (7), we obtain after some algebraic manipulation

$$\mathcal{M}[F_{\gamma_D}(\Theta x+\Theta-1),1-s]=\sum_{p}^{\infty}\frac{A_p}{2\pi j}\cdot\int_0^\infty\Gamma(1-s)\left(\frac{\Theta}{\Theta-1}\right)^{s-1}\cdot\int_{\mathcal{L}_2}\frac{\Gamma(1+p+\xi)\Gamma(-\xi)\Gamma(m_{s1}-\xi)\Gamma(\xi+s-1)}{\Gamma(1-\xi)\Gamma(\xi)}\left[\frac{(\Theta-1)(1+k_1)}{(m_{s1}-1)\overline{\gamma}_1}\right]^{-\xi}d\xi$$

$$\overset{(a)}{=}\sum_{p}^{\infty}A_p\cdot\frac{\Gamma(1-s)}{\left(\frac{\Theta}{\Theta-1}\right)^{1-s}}G_{3,3}^{2,2}\left(\frac{(\Theta-1)(1+k_1)}{(m_{s1}-1)\overline{\gamma}_1}\middle|\begin{matrix}1,1-m_{s1},0\\ 1-p,-(1+s),0\end{matrix}\right), \quad (9)$$

where (a) is based on the definition of Meijer G-function [7, Eq. (9.30)].

To solve the Mellin transform $\mathcal{M}[f_{\gamma_E}(x),s]=\int_0^\infty x^{s-1}f_{\gamma_E}(x)\,dx$, we utilize the result [6, Eq. (14)] and with some manipulations to obtain

$$\mathcal{M}[f_{\gamma_E}(x),s]\overset{(b)}{=}\frac{m_{d2}^{m_{d2}}\Gamma(m_{s2}-s+1)\Gamma(s)\cdot{}_2F_1\left(m_{d2},s;1;\frac{k_2}{(m_{d2}+k_2)}\right)}{(m_{d2}+k_2)^{m_{d2}}\Gamma(m_{s2})(1+k_2)^{s-1}[(m_{s2}-1)\overline{\gamma}_2]^{1-s}}$$

$$\overset{(c)}{=}\sum_{q=0}^{\infty}\underbrace{\frac{\Gamma(m_{d2}+q)\left[\frac{k_2}{m_{d2}+k_2}\right]^q}{m_{d2}^{-m_{d2}}\left[\Gamma(q+1)\right]^2(m_{d2}+k_2)^{m_{d2}}\Gamma(m_{s2})\Gamma(m_{d2})}}_{B_q}\cdot\frac{\Gamma(m_{s2}-s+1)}{[\Gamma(s+q)]^{-1}}\left[\frac{(m_{s2}-1)\overline{\gamma}_2}{1+k_2}\right]^{s-1}$$

$$=\sum_{q=0}^{\infty}B_q\cdot\frac{\Gamma(m_{s2}-s+1)}{[\Gamma(s+q)]^{-1}}\left[\frac{(m_{s2}-1)\overline{\gamma}_2}{1+k_2}\right]^{s-1}, \quad (10)$$

where (b) follows by change of random variable in [6, Eq. (14)] and (c) is obtained by first expressing the Gauss hypergeometric function in series [7, Eq. (9.14)] and using the definition of Pochhammer symbol [7, p. xli].

Next, substituting (9) and (10) into (6), we obtain

$$SOP = \left(\frac{1}{2\pi j}\right)^2 \frac{(\Theta-1)(1+k_2)}{\Theta(m_{s2}-1)\overline{\gamma}_2} \sum_{p=0}^{\infty}\sum_{q=0}^{\infty} A_p \cdot B_q \int_{\mathcal{L}_1}\int_{\mathcal{L}_2} \Gamma(m_{s2}-s+1) \cdot \frac{\Gamma(1-s)\Gamma(s+q)\Gamma(1+p+\xi)\Gamma(-\xi)\Gamma(m_{s1}-\xi)\Gamma(\xi+s-1)}{\Gamma(1-\xi)\Gamma(\xi)} \cdot \left[\frac{\Theta(m_{s2}-1)\overline{\gamma}_2}{(\Theta-1)(1+k_2)}\right]^s \left[\frac{(m_{s1}-1)\overline{\gamma}_1}{(\Theta-1)(1+k_1)}\right]^{\xi} d\xi ds. \quad (11)$$

Recalling the representation of bivariate Meijer G-function in terms of double contour integral [10, Table I] in (11), the exact expression for the SOP can be expressed in terms of bivariate Meijer G-function as

$$SOP = \frac{(\Theta-1)(1+k_2)}{\Theta(m_{s2}-1)\overline{\gamma}_2} \cdot \sum_{p=0}^{\infty}\sum_{q=0}^{\infty} A_p \cdot B_q \cdot G_{1,0:2,3:1,2}^{1,0:2,1:2,1}\left(\begin{matrix}-1\\-\end{matrix}\middle|\begin{matrix}-p,1\\0,m_{s1},1\end{matrix}\middle|\begin{matrix}1-q\\1,1+m_{s2}\end{matrix}\middle|\frac{(m_{s1}-1)\overline{\gamma}_1}{(\Theta-1)(1+k_1)}, \frac{\Theta(m_{s2}-1)\overline{\gamma}_2}{(\Theta-1)(1+k_2)}\right), \quad (12)$$

where the bivariate Meijer G-function can be efficiently evaluated in terms of double contour integral with numerical softwares such as Matlab and Mathematica [10, Table II].

PNZSC analysis: The PNZSC is a fundamental metric to evaluate the system secrecy performance that indicates the probability of transmission with (strictly positive) secrecy capacity [11]. We may write PNZSC as

$$PNZSC = \Pr\left[\gamma_D > \gamma_E\right] = 1 - \int_0^{\infty} F_{\gamma_D}(x) f_{\gamma_E}(x)\, dx. \quad (13)$$

The PNZSC in (13) can be solved by first substituting [7, Eq. (9.14)] in the PDF $f_{\gamma_E}(x)$, applying the property [12, Eq. 8.4.2.5], then solving the resultant integral with [12, Eq. 2.24.1], and simplifying, we obtain

$$PNZSC = 1 - \sum_{p=0}^{\infty}\sum_{q=0}^{\infty} \frac{A_p m_{s2} m_{d2}^{m_{d2}} (m_{d2})_q (m_{s2}+1)_q k_2^q}{(q!)^2 \Gamma(m_{s2}+q+1)(m_{d2}+k_2)^{m_{d2}+q}} \cdot G_{3,3}^{2,3}\left(\frac{(1+k_1)(m_{s2}-1)\overline{\gamma}_2}{(m_{s1}-1)(1+k_2)\overline{\gamma}_1}\middle|\begin{matrix}1,1-m_{s1},-q\\p+1,m_{s2},0\end{matrix}\right). \quad (14)$$

Numerical analysis and discussions: Figures 1 and 2 show the calculated SOP for varying values of shadowing parameters m_d and m_s under different values of Rician k parameter. For the evaluation purpose, the target secrecy rate is set as $R_s = 1$ nat/s/Hz. It is obvious from the analytical results in Figs. 1 and 2 that the multiplicative shadowing parameter m_s has a larger impact on the SOP than the LoS shadowing parameter m_d (even when the Rician k factor is relatively large). Also, it is observed that the SOP performance degrades faster when the shadowings become severer. The concept of "protected zone" around the legitimate transmitter was initially proposed to enhance the secrecy by decreasing the capacity of wiretap channel [1]. Due to the very destructive effect of multiplicative shadowing resulting from the obstacles in the vicinity of the receiver, it is also necessary that the "protected zone" is applied for the legitimate receiver to diminish the adverse effect of multiplicative shadowing caused by the obstructing objects around it (thus leading to larger m_s).

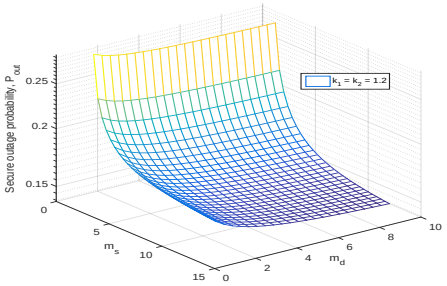

Fig. 1 *SOP versus shadowing parameters m_d and m_s*
$m_{d1} = m_{d2} = m_d$, $m_{s1} = m_{s2} = m_s$, $\overline{\gamma}_1 = 15$ dB, and $\overline{\gamma}_2 = 5$ dB

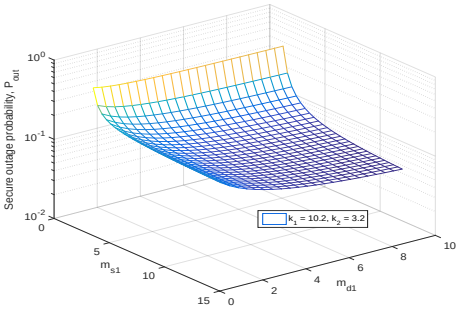

Fig. 2 *SOP versus shadowing parameters m_{d1} and m_{s1}*
$m_{d2} = 3.2$, $m_{s2} = 3.2$, $\overline{\gamma}_1 = 15$ dB, and $\overline{\gamma}_2 = 5$ dB

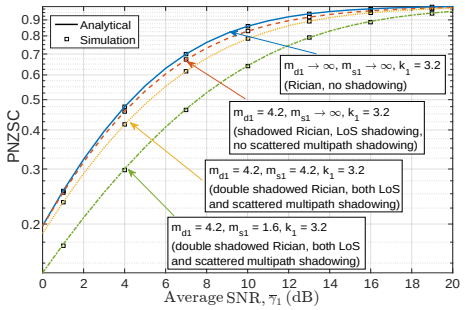

Fig. 3 *PNZSC versus average SNR $\overline{\gamma}_1$*
$m_{d2} = 4.2$, $m_{s2} = 4.2$, $k_2 = 6.2$, and $\overline{\gamma}_2 = 5$ dB

Figure 3 shows the PNZSC in terms of average SNR $\overline{\gamma}_1$ under different shadowing conditions. The results in Fig. 3 reaffirms previous analysis on the impact of two different types of shadowings on secrecy performance.

The G-functions are evaluated using Mathematica with high precision, and the infinite series in each expression are truncated to the same finite number of $\mathcal{N} = 20$ terms, resulting in a sufficiently small truncation error.

Conclusion: In this paper, we derive novel and exact expressions for the SOP and PNZSC for the PLS over the newly proposed double shadowed Rician fading channels. The results provide insights as well as physical implications on the impact of shadowings on secrecy performance.

Y. Ai and M. Cheffena (*Faculty of Engineering, Norwegian University of Science and Technology, 2815 Gjøvik, Norway*)
✉ E-mail: yun.ai@ntnu.no
L. Kong (*Department of Electrical Engineering, École de technologie supérieure, University of Québec, Montréal, QC H3C 1K3, Canada*)

References

1 F. Jameel *et al.*, "A comprehensive survey on cooperative relaying and jamming strategies for physical layer security," *IEEE Commun. Surveys Tuts.*, 2019, doi: 10.1109/COMST.2018.2865607.
2 Y. Ai *et al.*, "On physical layer security of double Rayleigh fading channels for vehicular communications," *IEEE Wireless Commun. Lett.*, vol. 7, no. 6, pp. 1038–1041, Dec. 2018.
3 H. Lei *et al.*, "On physical layer security over generalized Gamma fading channels," *IEEE Commun. Lett.*, vol. 19, no. 7, pp. 1257–1260, July 2015.
4 L. Kong and G. Kaddoum, "On physical layer security over the Fisher-Snedecor $\mathcal{F}$ wiretap fading channels," *IEEE Access*, vol. 6, pp. 39 466–39 472, July 2018.
5 N. Bhargav *et al.*, "Secrecy capacity analysis over κ-μ fading channels: Theory and applications," *IEEE Trans. Commun.*, vol. 64, no. 7, pp. 3011–3024, July 2016.
6 N. Bhargav *et al.*, "Double shadowing the Rician fading model," *IEEE Wireless Commun. Lett.*, vol. 8, no. 2, pp. 344–347, Apr. 2019.
7 I. S. Gradshteyn and I. M. Ryzhik, *Table of Integrals, Series, and Products*, 7th ed. Burlington, MA, USA: Academic Press, 2007.
8 Y. Ai *et al.*, "Secrecy performance analysis of wireless sensor networks," *IEEE Sensors Lett.*, vol. 3, no. 5, p. 4, May 2019.
9 A. D. Poularikas, *Transforms and Applications Handbook*. Boca Raton, FL, USA: CRC press, 2010.
10 I. S. Ansari *et al.*, "A new formula for the BER of binary modulations with dual-branch selection over Generalized-K composite fading channels," *IEEE Trans Commun.*, vol. 59, no. 10, Oct. 2011.
11 Y. Ai *et al.*, "Physical layer security of hybrid satellite-FSO cooperative systems," *IEEE Photon. J.*, vol. 11, no. 1, Feb. 2019.
12 A. Prudnikov *et al.*, *Integrals and Series. Volume 3: More Special Functions*. New York, NY, USA: Gordon and Breach Sci. Publ., 1986.